

# Localised H I 21-cm absorption towards a double-lobed $z = 0.24$ radio galaxy

S. J. Curran<sup>1\*</sup>, M. T. Whiting<sup>2</sup>, J. K. Webb<sup>1</sup> and R. Athreya<sup>3</sup>

<sup>1</sup>*School of Physics, University of New South Wales, Sydney NSW 2052, Australia*

<sup>2</sup>*CSIRO Australia Telescope National Facility, PO Box 76, Epping NSW 1710, Australia*

<sup>3</sup>*Indian Institute of Science Education and Research, 900, NCL Innovation Park, Dr Homi Bhabha Road Pune, Maharashtra 411008, India*

Accepted —. Received —; in original form —

## ABSTRACT

We present the results of a mini-survey for associated H I 21-cm absorption at  $z \leq 0.42$  with the Giant Metrewave Radio Telescope. Our targets are radio galaxies, selected on the basis that the  $\lambda \approx 1216 \text{ \AA}$  luminosities are below  $L_{\text{UV}} \sim 10^{23} \text{ W Hz}^{-1}$ , above which there has never been a detection of 21-cm absorption. Of the three sources for which we obtained good data, two are unclassified active galactic nuclei (AGN) and one is type-2. Being a non-detection, the type-2 object is consistent with our previous result that 21-cm absorption in radio sources is not dictated by unified schemes of AGN. In the case of the detection, the absorption only occurs towards one of the two resolved radio lobes in PKS 1649–062. If the absorption is due to another intervening galaxy, or cool H I gas in the intergalactic medium, covering only the south-west lobe, then, being at the same redshift, this is likely to be gravitationally bound to the optical object identified as PKS 1649–062. If the absorption is due to an inclined disk centred between the lobes, intervening the SW lobe while being located behind the NE lobe, by assuming that it covers the emission peak at  $\approx 150 \text{ kpc}$  from the nucleus, we estimate a dynamical mass of  $\approx 3 \times 10^{12} M_{\odot}$  for the disk.

**Key words:** galaxies: active – quasars: absorption lines – radio lines: galaxies – ultra violet: galaxies – galaxies: fundamental parameters – galaxies: individual (PKS 1649–062)

## 1 INTRODUCTION

Redshifted H I 21-cm absorption can provide an excellent probe of the contents and nature of the early Universe, through surveys which are not subject to the same flux and magnitude limitations suffered by optical studies. In particular, observation of the epoch of re-ionisation (e.g. Carilli et al. 2004), measurement of the contribution of the neutral gas content to the mass density of the Universe (see Curran 2010), as well as measuring any putative variations in the values of the fundamental constants at large look-back times (Tzanavaris et al. 2005, 2007).

Such absorption is, however, currently rare, with only 75 H I 21-cm absorption systems at  $z \geq 0.1$  known – 41 of which occur in galaxies intervening the sight-lines to more distant quasars, with the remainder arising in the hosts of radio galaxies and quasars (summarised in Curran 2010; Curran & Whiting 2010, respectively).<sup>1</sup> While the 50% detection rate in intervening absorbers can be attributed to flux coverage effects, introduced by the geometry of a flat expanding Universe (Curran & Webb 2006; Curran et al. 2010), the detection rate in these latter “associated” systems is currently attributed to unified schemes of active galactic nuclei (AGN),

where only type-2 objects present a dense column of absorbing gas along our sight-line. We (Curran et al. 2008b) have however recently found that the ultra-violet luminosity of the AGN is the key in determining whether 21-cm absorption is detected, with AGN type having little bearing on this, contrary to the current consensus (Gupta & Saikia 2006 and references therein). Indeed, UV luminosities may also be the root cause of other observed properties, seemingly responsible for the 21-cm detection rate in the hosts of radio galaxies and quasars (Curran & Whiting 2010 and verified by Grasha & Darling 2011).

We hence suggest that the paucity of redshifted 21-cm absorption is due to the optical selection of targets, where at such large distances only the most UV luminous are known. We have therefore embarked on several observing campaigns, at various redshifts, of optically faint sources in order to test this hypothesis and increase the number of associated 21-cm absorbers known at  $z \gtrsim 0.1$ . In this letter we present the first of these, a mini-survey using the 1000–1450 MHz band of the Giant Metrewave Radio Telescope (GMRT), in which we find 21-cm absorption towards one of the two lobes resolved in PKS 1649–062, a  $z = 0.24$  radio galaxy (Best et al. 1999).

\* E-mail: sje@phys.unsw.edu.au

<sup>1</sup> Adding a further two associated absorbers found by Curran et al. (2011).

## 2 THE 1420 MHz BAND GMRT MINI-SURVEY

### 2.1 Source selection

As per our previous surveys (Curran et al. 2006, 2008b, 2011), we selected targets from the Parkes Half-Jansky Flat-spectrum Sample (PHFS, Drinkwater et al. 1997), a source of bright and generally compact radio objects for which there exists comprehensive optical photometry (Francis et al. 2000). In order to ensure that the  $\lambda \approx 1216 \text{ \AA}$  luminosities of our targets are below the critical  $L_{\text{UV}} \sim 10^{23} \text{ W Hz}^{-1}$ , above which 21-cm has never been detected (Curran et al. 2008a), we target those which are sufficiently faint at a given redshift. However, applying the  $B - z$  curve (figure 5 of Curran et al. 2009) as an initial diagnostic, yields only two PHFS sources with  $B \gtrsim 22$  in the 307–347 MHz band ( $z = 3.09 - 3.63$ ), both of which have been previously searched for 21-cm (Curran et al. 2008b). Of the other available bands, there are three with  $B \gtrsim 20$  in the 580–640 MHz band ( $z = 1.22 - 1.45$ ), whereas in the 1000–1450 MHz band ( $z \lesssim 0.42$ ) there are 15 sources with measured redshifts and  $B \gtrsim 19$ .<sup>2</sup>

We therefore selected the ten faintest in this band, for which we also requested time to search for OH 18-cm absorption, on the basis of their large blue–near-infrared colours (all ten have  $B - K \geq 5.33$ , cf.  $\gtrsim 6$  for the five known redshifted OH absorbers, see Curran et al. 2011). However, time was only awarded to search for 21-cm in four objects and so we selected the two reddest which had not been previously searched, PKS 0036–216 ( $B - K = 6.22$ ) and 1128–047 ( $B - K = 7.55$ ), as well as the two with the largest flux densities (estimated to be  $\sim 2 \text{ Jy}$ ), 0153–410 and 1649–062.

### 2.2 Observations and data reduction

The four shortlisted targets (listed in Table 1) were observed with the 1000–1450 MHz receiver backed with the FX correlator over a bandwidth of 8 MHz split into 256 channels. This setup was chosen in order to give a channel spacing of  $\approx 8 \text{ km s}^{-1}$ , while maintaining a coverage of  $\Delta z \approx \pm 0.004$ , thus covering any uncertainties in the redshifts of the targets. Regarding the observations of these: **PKS 0036–216** was observed at a central frequency of 1061 MHz for a total of 0.90 hours on 26 November 2009. The delays were self calibrated, with PKS 0023–26 being used for the bandpass calibration. Minimal radio frequency interference (RFI) meant that only non-functioning antennas had to be flagged, leaving 365 good baseline pairs. For this, and the other targets, the data were reduced using the MIRIAD interferometry reduction package, from which a spectrum was extracted from the cube. The source was unresolved by the  $4.8'' \times 3.6''$  synthesised beam.

**PKS 0153–410** was observed at a central frequency of 1159 MHz for a total 1.82 hours on 26 November 2009. Again, the delays were self calibrated, with 3C 48 being used for bandpass calibration. Severe RFI over the length of the observation meant that no image could be produced.

**PKS 1128–047** was observed at a central frequency of 1122 MHz for a total of 0.93 hours on 25 July 2010. The delays were calibrated using LBQS 1148–0007 and the bandpass using 3C 286. RFI was minimal, leaving 365 good baseline pairs. The source was unresolved by the  $5.6'' \times 3.2''$  synthesised beam.

**PKS 1649–062** was observed at a central frequency of 1149 MHz

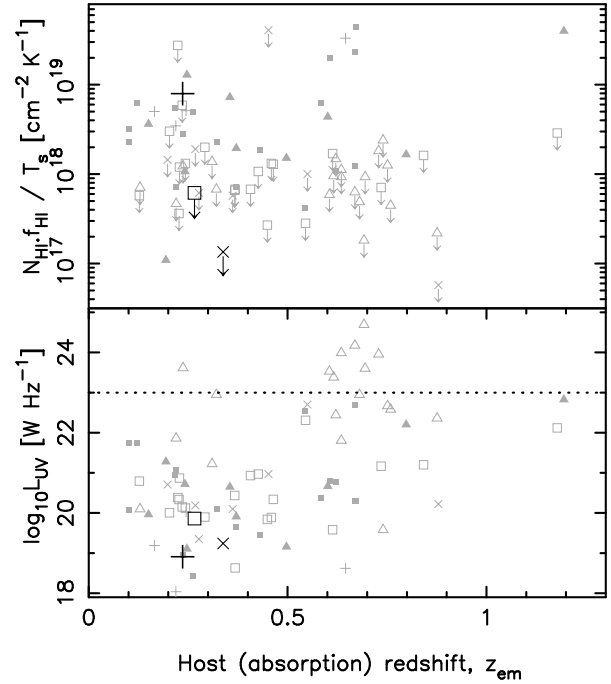


**Figure 2.** The scaled velocity integrated optical depth of the H I line ( $1.823 \times 10^{18} \cdot \int \tau dv$ ) [top] and the ultra-violet ( $\lambda \approx 1216 \text{ \AA}$ ) luminosity [bottom] versus the host redshift for the  $z \geq 0.1$  radio galaxies and quasars searched in associated 21-cm absorption. The filled symbols represent the 21-cm detections and the unfilled symbols the non-detections, with the large black symbols designating the new results presented here. The shapes represent the AGN classifications, with triangles representing type-1 objects and squares type-2s (+ and x designate an undetermined AGN type for a detection and non-detection, respectively). Limited to  $z \lesssim 1.2$  to show the new results. See Curran et al. (2011) for the full redshift range.

for a total of 2.29 hours on 27 November 2009. The delays were calibrated using PKS 1621–11, with bandpass calibration by 3C 273 and 3C 468. Although there was little sign of RFI, after calibration, using either bandpass calibrator, some of the antenna pairs (involving mostly antenna number 15 and above) exhibited flux densities which were so low as to be comparable with the r.m.s. noise and the inclusion of these prevented the production of any reasonable image. We therefore used a script to automatically flag all of those with a mean flux-to-noise ratio below some specified value. Only once this value reached 10 was a reasonable image (that shown in Fig. 1, left) obtained and since this left us with only 60 baseline pairs, further flagging would have been detrimental to this. The flagging of the longer baselines meant that the synthesised beam was much coarser than for the other observations ( $50'' \times 29''$ ). Nevertheless, this was sufficient to resolve a double lobed radio source, in which 21-cm absorption was detected towards one of the lobes.

## 3 RESULTS AND DISCUSSION

### 3.1 Survey results

In Table 1 we summarise the results of the survey, where we detected 21-cm in one of the three sources for which there are useful data (see Fig. 1, right). Showing the limits obtained in the top panel of Fig. 2, we see that the column density of the detection is in the nominal range of those previously searched and that the two non-detections are at comparatively deep limits. In the bottom panel we

<sup>2</sup> Although  $B \gtrsim 17$  should be close to ensuring  $L_{\text{UV}} \lesssim 10^{23} \text{ W Hz}^{-1}$  at these redshifts (Curran et al. 2009).

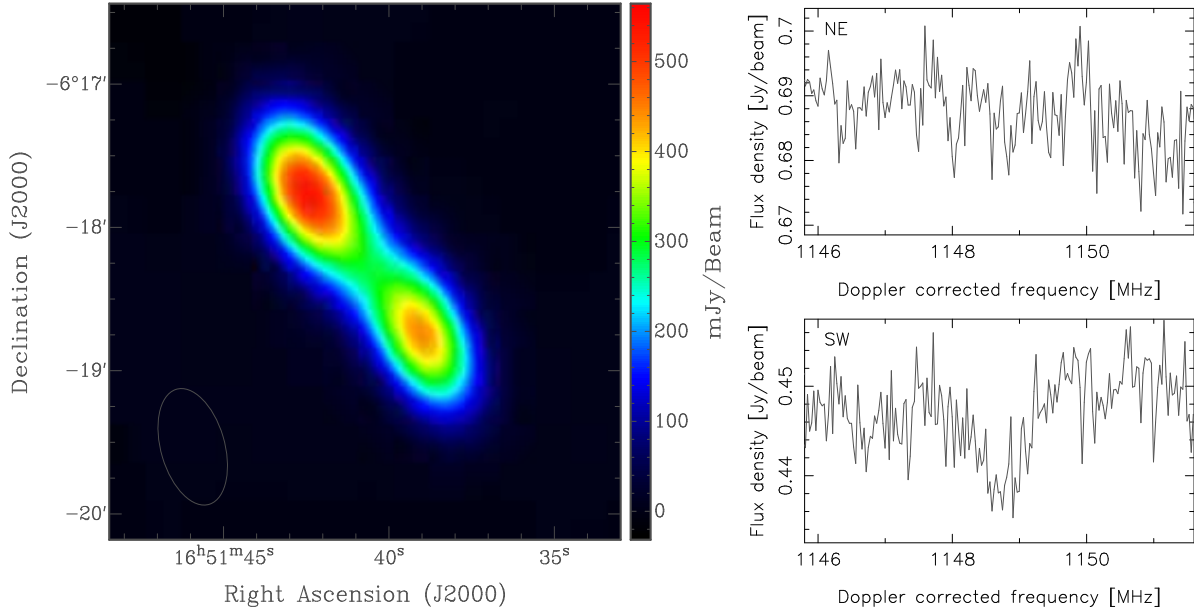


**Figure 1.** Left: The GMRT 1149 MHz continuum image of PKS 1649–062 (cf. the 408 MHz image of Best et al. 1999, which also resolves the two features). The beam is shown in the bottom left corner. Right: The spectra extracted from the north-east and south-west lobes of the image, shown at the observed channel width of  $8.2 \text{ km s}^{-1}$ .

**Table 1.** Summary of the search for 21-cm absorption in the hosts of optically faint PHFS sources which fall into the 1000–1450 MHz band.  $\nu_{\text{obs}}$  is the observed central frequency [MHz],  $B$  is the blue magnitude used in the selection of the sources,  $L_{\text{UV}}$  is the  $\lambda = 1216 \text{ \AA}$  luminosity of the target [ $\text{W Hz}^{-1}$ ] (calculated using the method prescribed in Curran et al. 2008b),  $\sigma_{\text{rms}}$  is the r.m.s. noise [mJy/beam] reached per  $\Delta v$  channel [ $\text{km s}^{-1}$ ],  $S_{\text{cont}}$  is the continuum flux [Jy],  $\tau$  is the peak optical depth of the line, where  $\tau = -\ln(1 - 3\sigma_{\text{rms}}/S_{\text{cont}})$  is quoted for the non-detections,  $N_{\text{HI}}$  is the resulting column density [ $\text{cm}^{-2}$ ], where  $T_s/f$  is the spin temperature/covering factor degeneracy of the of 21-cm absorbing gas, followed by the redshift range over which this applies. Finally, we give the AGN type.

PKS	$z_{\text{em}}$	$\nu_{\text{obs}}$	$B$	$\log_{10} L_{\text{UV}}$	$\sigma_{\text{rms}}$	$\Delta v$	$S_{\text{cont}}$	$\tau$	$N_{\text{HI}}$	$z$ -range	Type
0036–216	0.338	1061	21.20	19.24	2.3	8.8	0.67	$< 0.010$	$< 1.7 \times 10^{17} \cdot (T_s/f)$	0.3325–0.3425	–
0153–410	0.226	1159	19.81	19.67	—	8.1	—	RFI DOMINATED			2
1128–047	0.266	1122	21.41	19.86	4.1	8.4	0.31	$< 0.040$	$< 6.1 \times 10^{17} \cdot (T_s/f)$	0.2615–0.2705	2
1649–062											
NE	0.236	1149	20.44	18.91	5.1	8.2	0.69	$< 0.022$	$< 3.3 \times 10^{17} \cdot (T_s/f)$	0.2319–0.2395	–
SW	...	...	...	...	4.1	...	0.45	0.029	$8 \pm 2 \times 10^{18} \cdot (T_s/f)$	0.23647	...

show how the  $\lambda = 1216 \text{ \AA}$  luminosities of our targets compare to those previously searched for 21-cm absorption, where, as expected from our source selection, these are well below  $L_{\text{UV}} \sim 10^{23} \text{ W Hz}^{-1}$ , at the lower end of the searched UV range.

As discussed in Sect. 1, the detection of 21-cm absorption in radio galaxies and quasars is usually attributed to unified schemes of AGN, where type-2 objects generally exhibit absorption, whereas type-1 objects do not. However, once the effect of the UV luminosity is removed, Curran et al. (2008b) found that there is a near 50% detection rate for *both* type-1 and type-2 objects. Unfortunately, two of the targets cannot be classified; 1649–062 does not have an AGN classification as its optical spectrum is purely that of an elliptical galaxy (Best et al. 1999), although it does have a Fanaroff & Riley (1974) type-II radio morphology, while 0036–216 does not have any published spectrum suitable for discerning its AGN type. The one non-detection for which there exists a classification (1128–0047, Table 1) is a type-2 object, which would be expected to exhibit absorption, where this determined by the unified schemes. Adding this to the statistics of the  $z \geq 0.1$  searches,

takes the detection rates to 11 out of 23 (48%) and 17 out of 38 (45%) for the type-1 and type-2 AGN, respectively.

### 3.2 The absorption in PKS 1649–062

We believe that this is the highest redshift detection of H I 21-cm absorption against an extended radio lobe to date, the first cases being 3C 234 ( $z = 0.185$ , Pihlström 2001) and Coma A ( $z = 0.086$ , Morganti et al. 2002). In Fig. 3 we show the Gaussian fit to the absorption profile of 1649–062. The full-width half maximum (FWHM) of  $181 \text{ km s}^{-1}$  gives a velocity integrated line strength of  $1.91 \text{ Jy km s}^{-1}$ , which agrees well with the  $2.0 \pm 0.5 \text{ Jy km s}^{-1}$  obtained from summing the channels. The peak absorption occurs at a velocity offset of  $116 \text{ km s}^{-1}$  from the reference  $z = 0.236$  (with a depth of 10 mJy), which gives a redshift of  $z = 0.23648$ . This is consistent, within uncertainties, with the  $z = 0.236 \pm 0.002$  obtained from the optical spectrum (Best et al. 1999). From the image, the centre of the NE and SW emission regions are separated by  $\approx 80''$  (both  $\approx 40''$  from the point of mini-

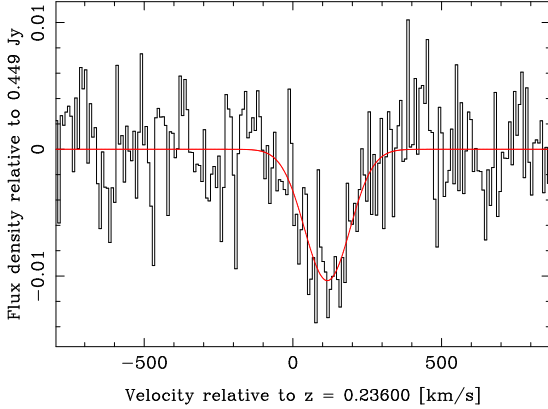


**Figure 3.** Gaussian fit to the absorption towards the SW lobe.

mum flux), which gives a projected extent of  $\approx 300$  kpc spanning between both emission peaks.<sup>3</sup>

### 3.2.1 Associated absorption by a large galactic disk

If the 21-cm absorption in PKS 1649–062 arises in a disk centred between the two radio lobes, it must have a non-negligible inclination along our sight-line in order to absorb in the SW, where it would occult the lobe, while being behind the NE lobe. For the disk to cover the peak emission at the SW lobe, its radius,  $r_{\text{disk}}$ , rotational velocity,  $v_{\text{disk}}$ , and inclination,  $i$ , would be related to the observed properties via

$$r_{\text{disk}} \geq \left( \frac{v_{\text{disk}}}{v_{\text{obs}}} \right) \left( \frac{r_{\text{lobe}}}{\tan i} \right), \quad (1)$$

where  $r_{\text{lobe}}$  is the projected distance of the emission peak from the nucleus and  $v_{\text{obs}}$  is the observed rotational velocity. Although we do not have the information to break the degeneracy, combining equation 1 with Newton’s second law gives for the dynamical mass, in solar masses,

$$M_{\text{dyn}} \geq 231 \left( \frac{v_{\text{obs}}}{r_{\text{lobe}}} \right)^2 r_{\text{disk}}^3 \tan^2 i, \quad (2)$$

where  $r_{\text{disk}}$  [pc] is the disk radius rotating at  $v_{\text{disk}}$  [km s<sup>−1</sup>].

Applying  $r_{\text{lobe}} \approx 150$  kpc and the full observed line width of  $v_{\text{obs}} \approx \pm 160$  km s<sup>−1</sup>, in Fig. 4 we show the results of equations 1 and 2 for various disk inclinations, which are overlaid with the permitted velocity, radius and subsequent dynamical mass at various inclinations. These are constrained from  $r_{\text{disk}} = r_{\text{lobe}}/\sin i$  and  $v_{\text{disk}} = (r_{\text{disk}}/r_{\text{em}})(v_{\text{obs}}/\cos i)$ , where  $r_{\text{em}}$  is the extent of the background emission behind the disk. We find this to be  $\approx 200$  kpc (beyond which the summed continuum and absorption profile disappear). The additional factor of  $r_{\text{disk}}/r_{\text{em}}$  is used to account for the possibility that the observed velocity, in addition to being projected in inclination, may be a projection due to the background emission not reaching as far as the disk edge, thus not allowing this to absorb. That is, this correction accounts for the possibility that the 21-cm absorption may not extend as far as the 21-cm emission from the disk, could this be detected. Note that the correction is responsible for the climb in velocity above  $r_{\text{disk}} \approx 200$  kpc in Fig. 4, where otherwise this would decline to close to the observed

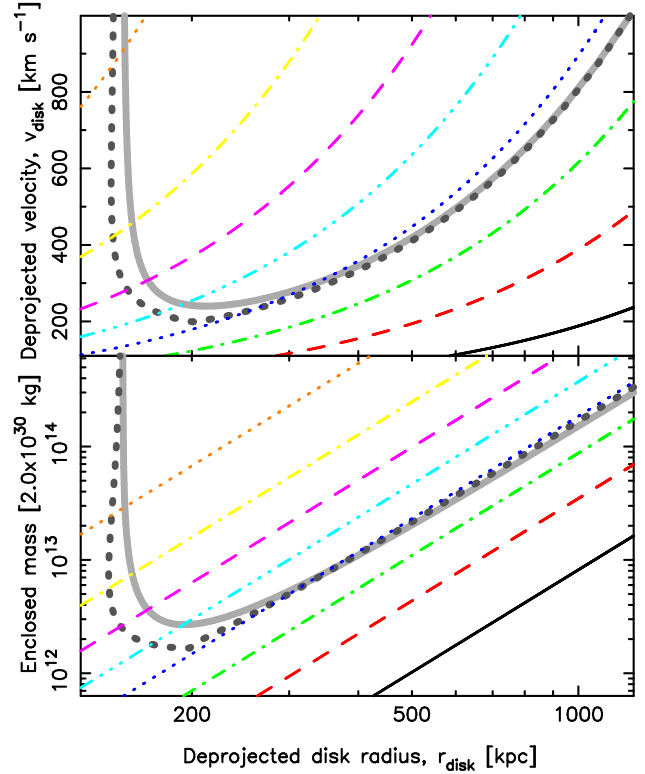


**Figure 4.** The deprojected rotation velocity (top) and dynamical mass (bottom) versus radius for a disk with an observed maximum rotational velocity of 160 km s<sup>−1</sup> and a projected radius of 150 kpc for various inclinations. The inclination angles decrease from left to right in steps of 10 degrees, starting at  $i = 80^\circ$  (dotted curve) and ending in  $i = 10^\circ$  (full curve). The thick contours show the permitted values for the putative disk at various inclinations (full for a thin disk and broken for a thick disk, see main text).

velocity by a radius of  $\gtrsim 1$  Mpc (where  $v_{\text{disk}} \lesssim 162$  km s<sup>−1</sup> and  $i \lesssim 9^\circ$ ).

From this model, we find a minimum mass of  $2.7 \times 10^{12} M_\odot$  (for  $i \approx 50^\circ$ , where  $v_{\text{disk}} \approx 240$  km s<sup>−1</sup> and  $r_{\text{disk}} \approx 200$  kpc). Without a maximum deprojected velocity we cannot estimate the maximum possible dynamical mass, but adopting the  $\pm 290$  km s<sup>−1</sup>, which is the largest profile width found in the low redshift ( $z \lesssim 0.04$ ) HI Parkes All-Sky Survey (Koribalski et al. 2004), gives a dynamical mass of  $3.3 \times 10^{12} M_\odot$  within a 170 kpc radius ( $i \approx 60^\circ$ , from the  $r_{\text{disk}} \leq r_{\text{em}}$  part of the curve).

Large (100 kpc-scale) disks have been observed in near-by radio galaxies (e.g. Morganti et al. 2002; Emonts et al. 2008) and, in order to account for the asymmetric properties observed in some radio galaxies, “superdisks” of gas and dust around the elliptical hosts of powerful radio galaxies, have been proposed. These are oriented roughly orthogonal to the radio jets, where one lobe is obscured by the disk (Athreya et al. 1998; Gopal-Krishna & Wiita 2000). Such disks have diameters of at least 75 kpc, although the maximum in the sample of Gopal-Krishna & Wiita (2000) is 137 kpc, which is considerably lower than the minimum estimated diameter of  $\approx 340$  kpc for the putative disk in PKS 1649–062. These superdisks can be one third as thick as they are long and broadening the disk to this ratio with the addition of a  $(t_{\text{disk}}/2) \cos i$  term, where  $t_{\text{disk}}$  is the disk thickness, and assuming no shear across the edge of the disk (Fig. 4, broken contours), still gives a diameter of  $\gtrsim 300$  kpc ( $i \lesssim 56^\circ$  and  $M_{\text{dyn}} \approx 2.7 \times 10^{12} M_\odot$ , for  $r_{\text{disk}} \leq r_{\text{em}}$ ) for  $v_{\text{disk}} \lesssim 290$  km s<sup>−1</sup>.

<sup>3</sup> For  $H_0 = 71$  km s<sup>−1</sup> Mpc<sup>−1</sup>,  $\Omega_{\text{matter}} = 0.27$  and  $\Omega_\Lambda = 0.73$ .



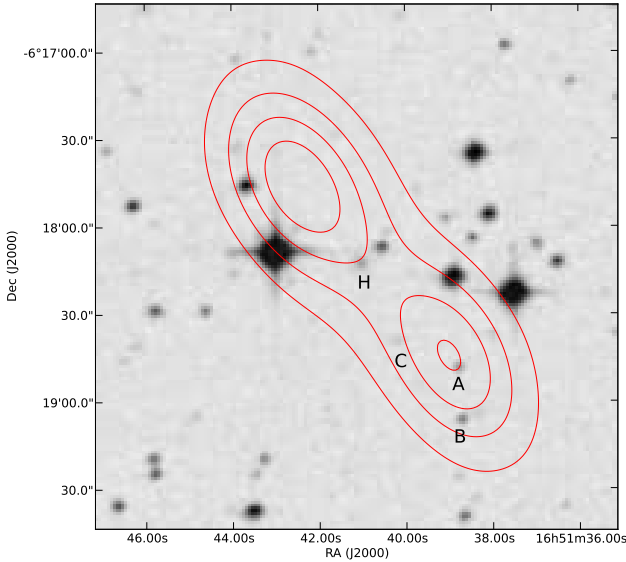


**Figure 5.** The 1149MHz continuum emission overlaid on a red POSS2 optical image. The host galaxy, as determined by Best et al. (1999), is labelled 'H', with three potential hosts for the absorbing gas labelled 'A', 'B' and 'C' (see main text for description).

**Table 2.** The  $B$  and  $R$  magnitudes of the possible absorption features.

	$B$	$R$	$B - R$		$B$	$R$	$B - R$
H	20.44	17.43	3.01	B	19.76	17.95	1.81
A	20.13	18.75	1.38	C	—	19.67	—

### 3.2.2 Other possible sources of absorption

Such a large implied size for a single absorbing disk can be avoided by having the absorbing gas:

(i) *Within or close to a neighbouring galaxy.* Referring to an optical image of the field (Fig. 5), there are at least three candidates for the location of the absorbing gas lying within the SW radio lobe (A, B and C), although the absorption redshift would require the gas to be located in the same cluster as the host, 'H', which is the only galaxy in this field with a known redshift (Best et al. 1999). We list the photometry of the host and the three candidate objects in Table 2 using the USNO-B survey (Monet et al. 2003), from which we see that the colours ( $B - R$ ) of 'A' and 'B' are not as red as the host galaxy. Without spectroscopy, however, it is unclear whether this difference is due to a difference in redshift, or whether they lack the 4000Å break of the host galaxy (Best et al. 1999).

(ii) *Arising from tidal debris left over from a major merger event.* The presence of 21-cm absorption as far as  $\approx 150$  kpc from the nucleus may be naturally explained by the cold gas left over from a collision, a common mechanism in the formation of powerful radio galaxies (Heckman et al. 1986; Baum et al. 1992). The component of this debris which remains gravitationally bound may eventually form a large H I disk structure on the time-scale of a Gyr (e.g. Barnes 2002; Morganti et al. 2002; Emonts et al. 2006).

(iii) *Cool gas in the intergalactic medium (IGM).* Pihlström (2001) describes a similar situation to that of PKS 1649–062, where 21-cm absorption is detected primarily towards one of the two lobes in 3C 234. This is interpreted as cool gas in the IGM, possibly

where the radio lobe interacts with this, and so may also explain the localised absorption we observe.

## ACKNOWLEDGEMENTS

We would like to thank Anant Tanna for the digitised 21-cm spectrum of NGC 0134 from Koribalski et al. (2004). This research has made use of the NASA/IPAC Extragalactic Database (NED) which is operated by the Jet Propulsion Laboratory, California Institute of Technology, under contract with the National Aeronautics and Space Administration. This research has also made use of NASA's Astrophysics Data System Bibliographic Services.

## REFERENCES

- Athreya R. M., Kapahi V. K., McCarthy P. J., van Breugel W., 1998, *A&A*, 329, 809
- Barnes J. E., 2002, *MNRAS*, 333, 481
- Baum S. A., Heckman T. M., van Breugel W., 1992, *ApJ*, 389, 208
- Best P. N., Röttgering H. J. A., Lehnert M. D., 1999, *MNRAS*, 310, 223
- Carilli C. L., Gnedin N., Furlanetto S., Owen F., 2004, *Science with the Square Kilometer Array*, New Astronomy Reviews 48. Elsevier, Amsterdam, pp 1053–1061
- Curran S. J., 2010, *MNRAS*, 402, 2657
- Curran S. J., Tzanavaris P., Darling J. K., Whiting M. T., Webb J. K., Bignell C., Athreya R., Murphy M. T., 2010, *MNRAS*, 402, 35
- Curran S. J., Webb J. K., 2006, *MNRAS*, 371, 356
- Curran S. J., Whiting M., Murphy M. T., et al., 2011, *MNRAS*, in press (arXiv:1012.1972)
- Curran S. J., Whiting M., Murphy M. T., Webb J. K., Longmore S. N., Pihlström Y. M., Athreya R., Blake C., 2006, *MNRAS*, 371, 431
- Curran S. J., Whiting M. T., 2010, *ApJ*, 712, 303
- Curran S. J., Whiting M. T., Webb J. K., 2008a, in *The Central Kiloparsec, Active Galactic Nuclei and Their Hosts Where is the cold neutral gas in the hosts of high redshift agn?*. *Memorie della Societa Astronomica Italiana*, Vol. 79, p. 1113
- Curran S. J., Whiting M. T., Webb J. K., 2009, *Proceedings of Science*, 89, Chap. 11
- Curran S. J., Whiting M. T., Wiklind T., Webb J. K., Murphy M. T., Purcell C. R., 2008b, *MNRAS*, 391, 765
- Drinkwater M. J., Webster R. L., Francis P. J., Condon J. J., Ellison S. L., Jauncey D. L., Lovell J., Peterson B. A., Savage A., 1997, *MNRAS*, 284, 85
- Emonts B., Morganti R., Oosterloo T., Holt J., Tadhunter C., van der Hulst J., Ojha R., Sadler E., 2008, *MNRAS*, 387, 197
- Emonts B. H. C., Morganti R., Tadhunter C. N., Holt J., Oosterloo T. A., van der Hulst J. M., Wills K. A., 2006, *A&A*, 454, 125
- Fanaroff B. L., Riley J. M., 1974, *MNRAS*, 167, 31P
- Francis P. J., Whiting M. T., Webster R. L., 2000, *PASA*, 17, 56
- Gopal-Krishna Wiita P. J., 2000, *ApJ*, 529, 189
- Grasha K., Darling J., 2011, in *American Astronomical Society Meeting Abstracts Vol. 217, A Search for Intrinsic HI 21-cm Absorption Toward Compact Radio Sources*. p. 345.02
- Gupta N., Saikia D. J., 2006, *MNRAS*, 370, 738
- Heckman T. M., Smith E. P., Baum S. A., Van Breugel W. J. M.,

- Miley G. K., Illingworth G. D., Bothun G. D., Balick B., 1986, *ApJ*, 311, 526
- Koribalski B. S., Staveley-Smith L., Kilborn V. A., et al., 2004, *AJ*, 128, 16
- Monet D. G., Levine S. E., Canzian B., et al., 2003, *AJ*, 125, 984
- Morganti R., Oosterloo T. A., Tinti S., Tadhunter C. N., Wills K. A., van Moorsel G., 2002, *A&A*, 387, 830
- Pihlström Y. M., 2001, PhD thesis, Chalmers University of Technology
- Tzanavaris P., Murphy M. T., Webb J. K., Flambaum V. V., Curran S. J., 2007, *MNRAS*, 374, 634
- Tzanavaris P., Webb J. K., Murphy M. T., Flambaum V. V., Curran S. J., 2005, *PhRvL*, 95, 041301